Two-nucleon transfer reactions as a test of quantum phase transitions in nuclei

Y. Zhang[1,2] and F. Iachello[1]

[1]*Center for Theoretical Physics, Sloane Physics Laboratory, Yale University, New Haven, Connecticut 06520-8120, USA*
[2]*Department of Physics, Liaoning Normal University, Dalian 116029, People's Republic of China*

A quantal and a semiclassical analysis of two-nucleon transfer intensities is done within the framework of the interacting boson model. The expected features of these quantities for the quantum phase transition (QPT) between spherical, U(5), and axially deformed, SU(3), shapes are discussed. Experimental data for (p,t) and (t,p) transfer reactions clearly show the occurrence of QPTs in Gd, Sm, and Nd.

I. INTRODUCTION

Quantum phase transitions (QPT) in nuclei have been, in recent years, the subject of many investigations [1–4]. QPTs are phase transitions that occur as a function of a parameter appearing in the quantum Hamiltonian describing the system. A class of QPTs found in nuclei is between two different shapes, hence the name "shape phase transitions" given to them. The two shapes (phases) have different symmetry. QPTs in nuclei acquired prominence when it was found that also at the critical point of the transition, a symmetry occurs, related to the scale invariance of the Hamiltonian [5,6]. An important question is to identify signatures of QPTs that can be tested by experiments. Several of these signatures have been discussed, including two-nucleon separation energies, $B(EL)$ values, isomer and isotope shifts, and energy ratios [1–4]. In this article, we discuss other signatures, related to two-neutron transfer intensities and show that experimental data in the rare-earth nuclei (Gd, Sm, and Nd) show evidence for a QPT connecting spherical and axially deformed shapes with symmetry U(5) and SU(3), respectively, thus confirming previous results obtained using other signatures [1–4,7]. The evolution of two-nucleon transfer intensities as a test of shape phase transitions within the framework of the interacting boson model (IBM) was previously given in the seminal work of [8], where the authors focused on discussing monopole two-nucleon transfer in (t,p) reactions. Here we enlarge the work of [8] by considering both monopole and quadrupole two-nucleon transfer in (t,p) and (p,t) processes, and most importantly, we do a wide and detailed comparison between theory and experiment.

The paper is divided in two parts. In the first part, we discuss the quantum and classical treatment of two-nucleon transfer reactions within the framework of the IBM [9]. In the second part, we perform a detailed analysis of available experimental data and show the evidence for QPT in Gd, Sm, and Nd.

II. TWO-NUCLEON TRANSFER INTENSITIES

In the IBM, two-neutron (ν) transfer operators corresponding to monopole-pair and quadrupole-pair are defined as [9,10]

$$P^{(0)}_{+,\nu,0} = t_{a_\nu} s^\dagger A(\Omega_\nu, N_\nu), \quad P^{(0)}_{-,\nu,0} = t_{a_\nu} A(\Omega_\nu, N_\nu) s, \quad (1)$$

$$P^{(2)}_{+,\nu,\mu} = t_{b_\nu} d^\dagger_\mu A(\Omega_\nu, N_\nu), \quad P^{(2)}_{-,\nu,\mu} = t_{b_\nu} A(\Omega_\nu, N_\nu) \tilde{d}_\mu \quad (2)$$

with the factor $A(\Omega_\nu, N_\nu)$ given by

$$A(\Omega_\nu, N_\nu) = \left(\Omega_\nu - N_\nu - \frac{N_\nu}{N} \hat{n}_d \right)^{\frac{1}{2}} \left(\frac{N_\nu + 1}{N + 1} \right)^{\frac{1}{2}}. \quad (3)$$

A similar expression holds for two-proton (π) transfer operators with the index ν replaced by π. In Eqs. (1) to (3), N_ν and Ω_ν represent the number of valence neutron (ν) pairs and their degeneracy, respectively, while t_{a_ν} and t_{b_ν} denote scale factors. Accordingly, the (p,t) and (t,p) transfer intensities can be calculated as [9]

$$I^a(N+1, L' \to N, L)$$
$$= \frac{1}{2L'+1} |\langle N, L \| P_- \| N+1, L' \rangle|^2 \quad (4)$$

and

$$I^b(N, L \to N+1, L')$$
$$= \frac{1}{2L+1} |\langle N+1, L' \| P_+ \| N, L \rangle|^2, \quad (5)$$

respectively. We consider here those related to the lowest states with $L = 0$ and $L = 2$, specifically

$$I^a_1 = I(N+1, 0^+_1 \to N, 0^+_1), \quad (6)$$

$$I^a_2 = I(N+1, 0^+_1 \to N, 0^+_2), \quad (7)$$

$$I^a_3 = I(N+1, 0^+_1 \to N, 0^+_3), \quad (8)$$

$$I^a_4 = I(N+1, 0^+_1 \to N, 2^+_1), \quad (9)$$

$$I^a_5 = I(N+1, 0^+_1 \to N, 2^+_2), \quad (10)$$

$$I^a_6 = I(N+1, 0^+_1 \to N, 2^+_3), \quad (11)$$

for (p,t) reactions and

$$I^b_1 = I(N, 0^+_1 \to N+1, 0^+_1), \quad (12)$$

$$I^b_2 = I(N, 0^+_1 \to N+1, 0^+_2), \quad (13)$$

$$I^b_3 = I(N, 0^+_1 \to N+1, 0^+_3), \quad (14)$$

$$I^b_4 = I(N, 0^+_1 \to N+1, 2^+_1), \quad (15)$$

$$I_5^b = I(N, 0_1^+ \to N + 1, 2_2^+), \tag{16}$$

$$I_6^b = I(N, 0_1^+ \to N + 1, 2_3^+), \tag{17}$$

for (t,p) reactions.

A. Quantum treatment

We consider the Hamiltonian [11]

$$\hat{H}(\eta, \chi) = \varepsilon_0 \left[(1 - \eta)\hat{n}_d - \frac{\eta}{4N} \hat{Q}^\chi \cdot \hat{Q}^\chi \right], \tag{18}$$

where $\hat{Q}^\chi = (d^\dagger s + s^\dagger \tilde{d})^{(2)} + \chi (d^\dagger \tilde{d})^{(2)}$ is the quadrupole operator, η and χ are the control parameters with $\eta \in [0,1]$ and $\chi \in [-\sqrt{7}/2, 0]$, and ε_0 is a scale factor. This Hamiltonian can be used to study QPTs between all three phases of the IBM, with symmetry U(5) ($\eta = 0$), SO(6) ($\eta = 1$, $\chi = 0$), and SU(3) ($\eta = 1$, $\chi = -\sqrt{7}/2$). Here we study the QPT between U(5) and SU(3). Also, in nuclei, the control parameter is the nucleon number (or the boson number N), of which the value is discrete. To simulate a realistic situation, we use the parametrization [8]

$$\eta = 0.005N^2 - 0.125 \tag{19}$$

with η ranging from 0 to 1 when N creases from 5 to 15. The resulting difference between the initial and the final state is

$$\Delta \eta \equiv \eta(N + 1) - \eta(N)$$
$$= 0.01N + 0.005. \tag{20}$$

To study the behavior of the intensities and their classical limit, we consider in this section the matrix elements of s, d_μ [for the (p,t) reaction] and $s^\dagger$, $d_\mu^\dagger$ [for the (t,p) reaction]. For the quantum treatment, we calculate reduced matrix elements of these operators with wave functions obtained by diagonalizing $\hat{H}$ of Eq. (18).

B. Classical treatment

We introduce the boson condensates (coherent states) of IBM defined in [8,12,13] as

$$|N; g\rangle = \frac{1}{\sqrt{N!}} (B_g^\dagger)^N |0\rangle \tag{21}$$

with

$$B_g^\dagger = \frac{1}{\sqrt{1+\beta^2}} \left[s^\dagger + \beta \cos \gamma d_0^\dagger + \frac{1}{\sqrt{2}} \beta \sin \gamma (d_{-2}^\dagger + d_{+2}^\dagger) \right] \tag{22}$$

and, similarly

$$|N + 1; g'\rangle = \frac{1}{\sqrt{(N+1)!}} (B_{g'}^\dagger)^{N+1} |0\rangle \tag{23}$$

with

$$B_{g'}^\dagger = \frac{1}{\sqrt{1+\beta'^2}} \left[s^\dagger + \beta' \cos \gamma' d_0^\dagger + \frac{1}{\sqrt{2}} \beta' \sin \gamma' (d_{-2}^\dagger + d_{+2}^\dagger) \right]. \tag{24}$$

In addition, we can define the β-vibrational state

$$|N + 1; \beta_v'\rangle = \frac{1}{\sqrt{(N+1)}} (B_{\beta_v'}^\dagger) B_{g'} |N + 1; g'\rangle \tag{25}$$

with

$$B_{\beta_v'}^\dagger = \frac{1}{\sqrt{1+\beta'^2}} \left[-\beta' s^\dagger + \cos \gamma' d_0^\dagger + \frac{1}{\sqrt{2}} \sin \gamma' (d_{-2}^\dagger + d_{+2}^\dagger) \right], \tag{26}$$

and the γ-vibrational state

$$|N + 1; \gamma_v'\rangle = \frac{1}{\sqrt{(N+1)}} (B_{\gamma_v'}^\dagger) B_{g'} |N + 1; g'\rangle \tag{27}$$

with

$$B_{\gamma_v'}^\dagger = \frac{1}{\sqrt{2}} \cos \gamma' (d_{+2}^\dagger + d_{-2}^\dagger) - \sin \gamma' d_0^\dagger. \tag{28}$$

In the case of axial symmetry ($\gamma = 0°$) the operator in Eq. (28) should be replaced with $B_{\gamma_v', \pm 2}^\dagger = d_{\pm 2}^\dagger$ to have a well-defined angular momentum projection on the symmetry axis [13]. One can also define double beta, $2\beta_v'$-vibrational state

$$|N + 1; 2\beta_v'\rangle = \frac{1}{\sqrt{2(N+1)N}} (B_{\beta_v'}^\dagger t)^2 (B_{g'})^2 |N + 1; g'\rangle. \tag{29}$$

By making use of [14]

$$[b_i, f(b)] = \frac{\partial}{\partial b_i^\dagger} f(b), \tag{30}$$

$$[f(b), b_i^\dagger] = \frac{\partial}{\partial b_i} f(b), \tag{31}$$

where b_i ($b_i^\dagger$) represents the annihilation (creation) operator for s or d boson, and $f(b)$ denotes a polynomial of b_i and $b_i^\dagger$, one can derive explicit formulas for matrix elements of $s^\dagger$ (s) and $d_\mu^\dagger$ (d_μ). They can be obtained one from the other using

$$\langle \phi' | b^\dagger | \phi \rangle = \langle \phi | b | \phi' \rangle. \tag{32}$$

$$(\mathbf{A}) \, \phi_g(N) \leftrightarrow \phi_g'(N+1)$$

For (t,p) or (p,t) transfer reactions between ground (g) bands, one can derive

$$\langle N; g | s | N + 1; g' \rangle$$
$$= \langle N + 1; g' | s^\dagger | N; g \rangle$$
$$= \frac{\sqrt{N+1}}{\sqrt{1+\beta'^2}} \left[\frac{1 + \beta\beta' \cos(\gamma - \gamma')}{\sqrt{(1+\beta'^2)(1+\beta^2)}} \right]^N, \tag{33}$$

$$\langle N; g | d_\mu | N + 1; g' \rangle$$
$$= \langle N + 1; g' | d_\mu^\dagger | N; g \rangle$$
$$= \frac{\sqrt{N+1}}{\sqrt{1+\beta'^2}} \left[\frac{1 + \beta\beta' \cos(\gamma - \gamma')}{\sqrt{(1+\beta'^2)(1+\beta^2)}} \right]^N$$
$$\times \left[\beta' \cos \gamma' \delta_{\mu,0} + \frac{1}{\sqrt{2}} \beta' \sin \gamma' (\delta_{\mu,2} + \delta_{\mu,-2}) \right]. \tag{34}$$

$$(\mathbf{B}) \, \phi_g(N) \to \phi_e'(N+1)$$

For the (t, p) transfer reaction between ground bands and excited (e) bands, one can find

$$\langle N+1; \beta_v'|s^\dagger|N; g\rangle = [N\beta\cos(\gamma-\gamma') - (N+1)\beta' - \beta\beta'^2\cos(\gamma-\gamma')]\frac{[1+\beta\beta'\cos(\gamma-\gamma')]^{N-1}}{(\sqrt{1+\beta^2})^N}\left(\frac{1}{\sqrt{1+\beta'^2}}\right)^{N+1}, \quad (35)$$

$$\langle N+1; \beta_v'|d_\mu^\dagger|N; g\rangle = \frac{[1+\beta\beta'\cos(\gamma-\gamma')]^{N-1}}{(\sqrt{1+\beta^2})^N}\left(\frac{1}{\sqrt{1+\beta'^2}}\right)^{N+1}\left\{[N\beta\beta'\cos\gamma\cos\gamma' - N\beta'^2 + 1 + \beta\beta'\cos(\gamma-\gamma')]\right.$$
$$\left. \times\left[\cos\gamma'\delta_{\mu,0} + \frac{1}{\sqrt{2}}\sin\gamma'(\delta_{\mu,2} + \delta_{\mu,-2})\right] + N\beta\beta'\sin\gamma\sin\gamma'\cos\gamma'\right\}, \quad (36)$$

$$\langle N+1; \gamma_v'|s^\dagger|N; g\rangle = N\beta\sin(\gamma-\gamma')\frac{[1+\beta\beta'\cos(\gamma-\gamma')]^{N-1}}{[\sqrt{(1+\beta^2)(1+\beta'^2)}]^N}, \quad (37)$$

$$\langle N+1; \gamma_v'|d_\mu^\dagger|N; g\rangle = \left[\frac{1+\beta\beta'\cos(\gamma-\gamma')}{\sqrt{(1+\beta^2)(1+\beta'^2)}}\right]^N\left[\frac{\cos\gamma'}{\sqrt{2}}(\delta_{\mu,2} + \delta_{\mu,-2})\right.$$
$$\left. - \sin\gamma'\delta_{\mu,0} + N\beta\sin(\gamma-\gamma')\frac{\beta'\cos\gamma'\delta_{\mu,0} + \frac{1}{\sqrt{2}}\beta'\sin\gamma'(\delta_{\mu,-2} + \delta_{\mu,2})}{1+\beta\beta'\cos(\gamma-\gamma')}\right], \quad (38)$$

$$\langle N+1; 2\beta_v'|s^\dagger|N; g\rangle = \sqrt{\frac{N}{2}}[\beta\cos(\gamma-\gamma') - \beta']\frac{[1+\beta\beta'\cos(\gamma-\gamma')]^{N-2}}{\sqrt{(1+\beta^2)^N(1+\beta'^2)^{N+1}}}$$
$$\times \{(N-1)[\beta\cos(\gamma-\gamma') - \beta'] - 2\beta'[1+\beta\beta'\cos(\gamma-\gamma')]\}, \quad (39)$$

$$\langle N+1; 2\beta_v'|d_\mu^\dagger|N; g\rangle = \sqrt{\frac{N}{2}}[\beta\cos(\gamma-\gamma') - \beta']\frac{[1+\beta\beta'\cos(\gamma-\gamma')]^{N-2}}{\sqrt{(1+\beta^2)^N(1+\beta'^2)^{N+1}}}\left[\cos\gamma'\delta_{\mu,0} + \frac{1}{\sqrt{2}}\sin\gamma'(\delta_{\mu,2} + \delta_{\mu,-2})\right]$$
$$\times \{2[1+\beta\beta'\cos(\gamma-\gamma')] + (N-1)\beta'[\beta\cos(\gamma-\gamma') - \beta']\}. \quad (40)$$

$$\text{(C)} \, \phi_g'(N+1) \to \phi_e(N)$$

For the (p, t) transfer reaction between ground bands and excited bands, one can find

$$\langle N; \beta_v|s|N+1; g'\rangle = \frac{[1+\beta\beta'\cos(\gamma-\gamma')]^{N-1}}{(\sqrt{1+\beta^2})^N}\left(\frac{1}{\sqrt{1+\beta'^2}}\right)^{N+1}\sqrt{N(N+1)}[\beta'\cos(\gamma-\gamma') - \beta], \quad (41)$$

$$\langle N; \beta_v|d_\mu|N+1; g'\rangle = \sqrt{N(N+1)}\frac{(1+\beta\beta'\cos(\gamma-\gamma'))^{N-1}}{(\sqrt{1+\beta^2})^N}\left(\frac{1}{\sqrt{1+\beta'^2}}\right)^{N+1}[\beta'\cos(\gamma-\gamma') - \beta]$$
$$\times\left[\beta'\cos\gamma'\delta_{\mu,0} + \frac{\beta'\sin\gamma'}{\sqrt{2}}(\delta_{\mu,2} + \delta_{\mu,-2})\right], \quad (42)$$

$$\langle N; \gamma_v|s|N+1; g'\rangle = \sqrt{N(N+1)}(\beta' + \beta^2\beta')\sin(\gamma'-\gamma)\frac{[1+\beta\beta'\cos(\gamma-\gamma')]^{N-1}}{[\sqrt{(1+\beta^2)(1+\beta'^2)}]^{N+1}}, \quad (43)$$

$$\langle N; \gamma_v|d_\mu|N+1; g'\rangle = \sqrt{(N+1)N(1+\beta^2)}\beta'\sin(\gamma'-\gamma)\left[\beta'\cos\gamma'\delta_{\mu,0} + \frac{1}{\sqrt{2}}\beta'\sin\gamma'(\delta_{\mu,2} + \delta_{\mu,-2})\right]$$
$$\times \frac{[1+\beta\beta'\cos(\gamma-\gamma')]^{N-1}}{(\sqrt{1+\beta^2})^N}\frac{1}{(\sqrt{1+\beta'^2})^{N+1}}, \quad (44)$$

$$\langle N; 2\beta_v|s|N+1; g'\rangle = \sqrt{\frac{(N+1)N(N-1)}{2}}[\beta'\cos(\gamma-\gamma') - \beta]^2\frac{[1+\beta\beta'\cos(\gamma-\gamma')]^{N-2}}{\sqrt{(1+\beta^2)^N(1+\beta'^2)^{N+1}}}, \quad (45)$$

$$\langle N; 2\beta_v|d_\mu|N+1; g'\rangle = \sqrt{\frac{(N+1)N(N-1)}{2}}[\beta'\cos(\gamma-\gamma') - \beta]^2\left[\beta'\cos\gamma'\delta_{\mu,0} + \frac{1}{\sqrt{2}}\beta'\sin\gamma'(\delta_{\mu,2} + \delta_{\mu,-2})\right]$$
$$\times \frac{[1+\beta\beta'\cos(\gamma-\gamma')]^{N-2}}{\sqrt{(1+\beta^2)^N(1+\beta'^2)^{N+1}}}. \quad (46)$$

The classical matrix elements of the s-boson operator for the (t,p) reactions shown in Eqs. (33), (35), and (39) had already been derived in [8]. Here we have given also those of the d boson and included the γ dependence for both (p,t) and (t,p) transfer reactions. We note that while for ground to ground transitions (A) there is no difference in the matrix elements for (p,t) and (t,p) reactions, for transitions between ground and excited bands there is a difference, already noted in ([9], p. 82), and for this reason we have given explicitly both in (B) and (C).

To connect the intensities of transfer reaction to QPTs, we return to the quantum Hamiltonian $\hat{H}$ of Eq. (18), and write down the potential energy surface corresponding to it

$$V(\beta,\gamma) \equiv \langle N; g|\hat{H}(\eta,\chi)|N; g\rangle$$

$$= \frac{\varepsilon_0 N\beta^2}{1+\beta^2}\left[(1-\eta) - (\chi^2+1)\frac{\eta}{4N}\right] - \frac{5\varepsilon_0\eta}{4(1+\beta^2)} - \frac{\varepsilon_0\eta(N-1)}{4(1+\beta^2)^2}\left[4\beta^2 - 4\sqrt{\frac{2}{7}}\chi\beta^3\cos3\gamma + \frac{2}{7}\chi^2\beta^4\right]. \quad (47)$$

This potential function can be used to study QPTs between all three phase of the IBM. To this end, one minimizes the potential function, Eq. (47), with respect to the quadrupole deformation parameters β and γ, obtaining the equilibrium classical order parameters, β_e and γ_e. The ground-state energy for a given value of η,χ is $E_g \equiv V(\eta,\chi,\beta_e,\gamma_e)$. It has been found that for the potential (47) either $\gamma_e = 0°$ ($\chi < 0$) or γ independent ($\chi = 0$). We henceforth set $\gamma = 0°$ and study only its β dependence.

In Fig. 1, we show the behavior of the order parameter β_e as a function of η for fixed N (or $N + 1$). This behavior is typical of a first-order transition, U(5)–SU(3), with a discontinuity in β_e, at the critical value η_c. The critical value is given by $\eta_c = 8/17$ for $N \to \infty$. Using the formulas (41) to (46) for $\gamma = \gamma' = 0°$ we can calculate the evolution of the matrix elements of s, d (or $s^\dagger$, $d_\mu^\dagger$) as a function of η. All of them appear to have discontinuities at $\eta = \eta_c$. In Figs. 2(a) to 2(d), we show the behavior of

$$F_1 \equiv |\langle N; g|s|N+1; g'\rangle|^2 = |\langle N+1; g'|s^\dagger|N; g\rangle|^2, \quad (48)$$

$$F_2 \equiv |\langle N; g|d_0|N+1; g'\rangle|^2 = |\langle N+1; g'|d_0^\dagger|N; g\rangle|^2, \quad (49)$$

$$F_3 \equiv |\langle N; \beta_v|s|N+1; g'\rangle|^2, \quad (50)$$

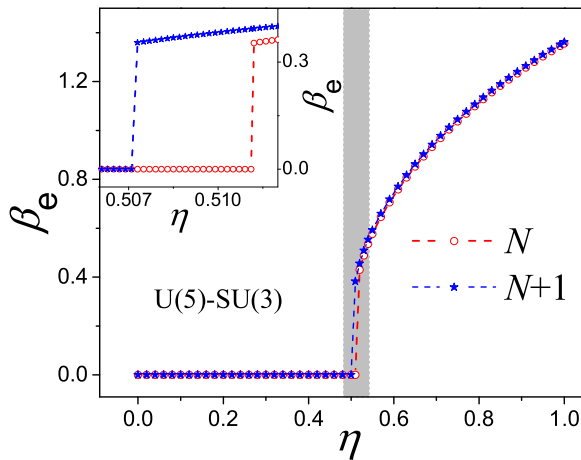$$F_4 \equiv |\langle N+1; \beta_v'|s^\dagger|N; g\rangle|^2 \quad (51)$$

FIG. 1. Evolution of the classical order parameter β_e in the U(5)–SU(3) transition for $N = 10$ with the inset showing the critical behavior of β_e.

as a function of η. These matrix elements are proportional to intensities of transfer (p,t) and (t,p) reactions $0_1^+ \to 0_1^+$, $0_1^+ \to 2_1^+$, and $0_1^+ \to 0_2^+$. Particularly important is the behavior of F_2 which is proportional to the square of the order parameter, β_e^2.

C. Quantal-classical correspondence

Since both the quantal and classical matrix elements can be calculated, it is of interest to study the quantal-classical correspondence. To this end, the quantal reduced matrix elements can be calculated as described in Sec. II A, while the classical matrix elements as described in Sec. II B. However, these last are calculated in the intrinsic frame and must be converted to the laboratory frame before making comparison. For a general tensor operator of rank λ, the conversion is given by

$$\langle I'M'K'|T_\mu^\lambda|IMK\rangle$$

$$= \sqrt{\frac{2I+1}{2I'+1}}\sqrt{\frac{1}{(1+\delta_{K,0})(1+\delta_{K',0})}}\langle IM\lambda\mu|I'M'\rangle$$

$$\times \sum_v \left[\langle IK\lambda v|I'K'\rangle\langle\phi_{K'}|T_v^\lambda|\phi_K\rangle\right.$$

$$\left. + (-)^{I+K}\langle I-K\lambda v|I'K'\rangle\langle\phi_{K'}|T_v^\lambda|\phi_{\overline{K}}\rangle\right], \quad (52)$$

which yields, using the Wigner-Eckart theorem,

$$\langle I'K'||T^\lambda||IK\rangle$$

$$= \sqrt{\frac{2I+1}{(1+\delta_{K,0})(1+\delta_{K',0})}}\sum_v\left[\langle IK\lambda v|I'K'\rangle\langle\phi_{K'}|T_v^\lambda|\phi_K\rangle\right.$$

$$\left. + (-)^{I+K}\langle I-K\lambda v|I'K'\rangle\langle\phi_{K'}|T_v^\lambda|\phi_{\overline{K}}\rangle\right]. \quad (53)$$

The quantal-classical correspondence is shown in Figs. 3 and 4.

From these figures one can see that the quantal and classical matrix elements of the operators s and $s^\dagger$ are in close correspondence to each other. The matrix elements of the operator d and $d^\dagger$ in the ground band are also in close correspondence to each other, but those in the excited bands are in close correspondence in the deformed phase, $N = 11 - 14$, but not in the spherical phase, $N = 5 - 10$ as shown in Figs. 4(e) and 4(f). This is due to the fact that the intrinsic states, Eqs. (25) and (27), describing β and γ vibrations are appropriate only in the deformed phase. Moreover, in Fig. 4(d),
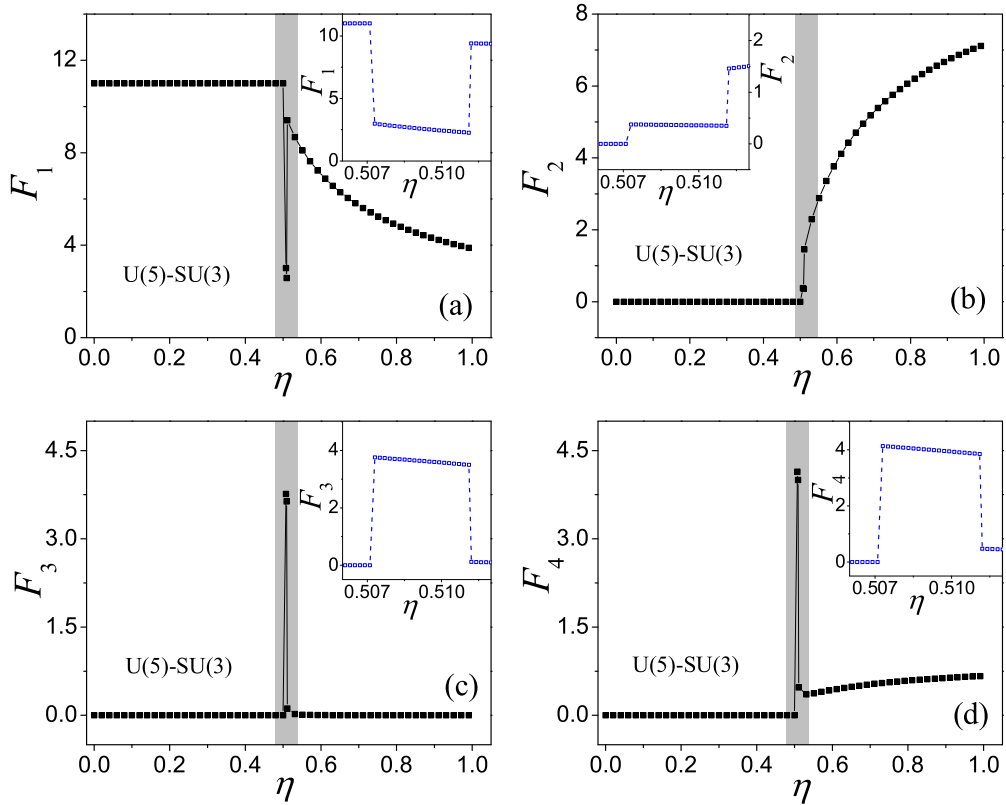
FIG. 2. (a) Evolution of the classical element F_1 in the U(5)–SU(3) transition for $N = 10$ with the inset showing the behavior in the vicinity of the critical point. (b) The same as in (a) but for F_2. (c) The same as in (a) but for F_3. (d) The same as in (a) but for F_4.
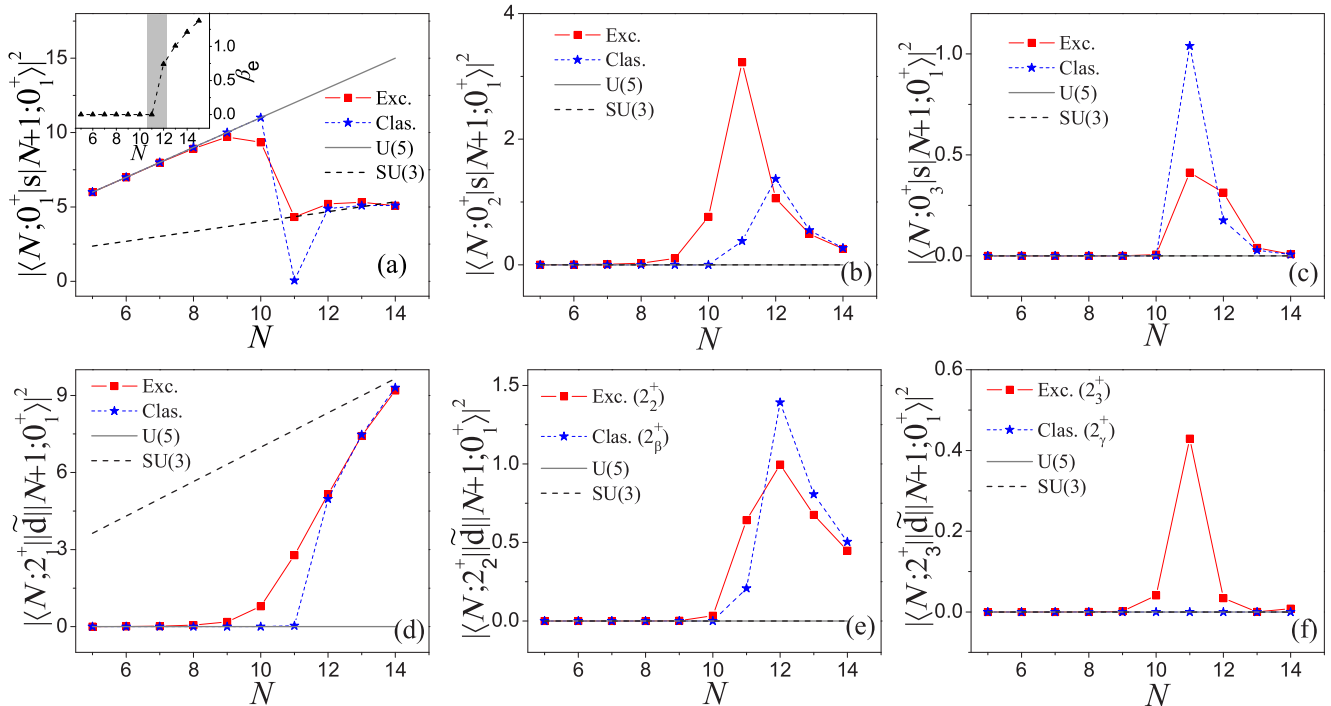

FIG. 3. Quantal-classical correspondence for the matrix elements of s, d_μ appropriate to (p,t) reaction intensities. The inset in panel (a) shows the critical behavior of β_e.
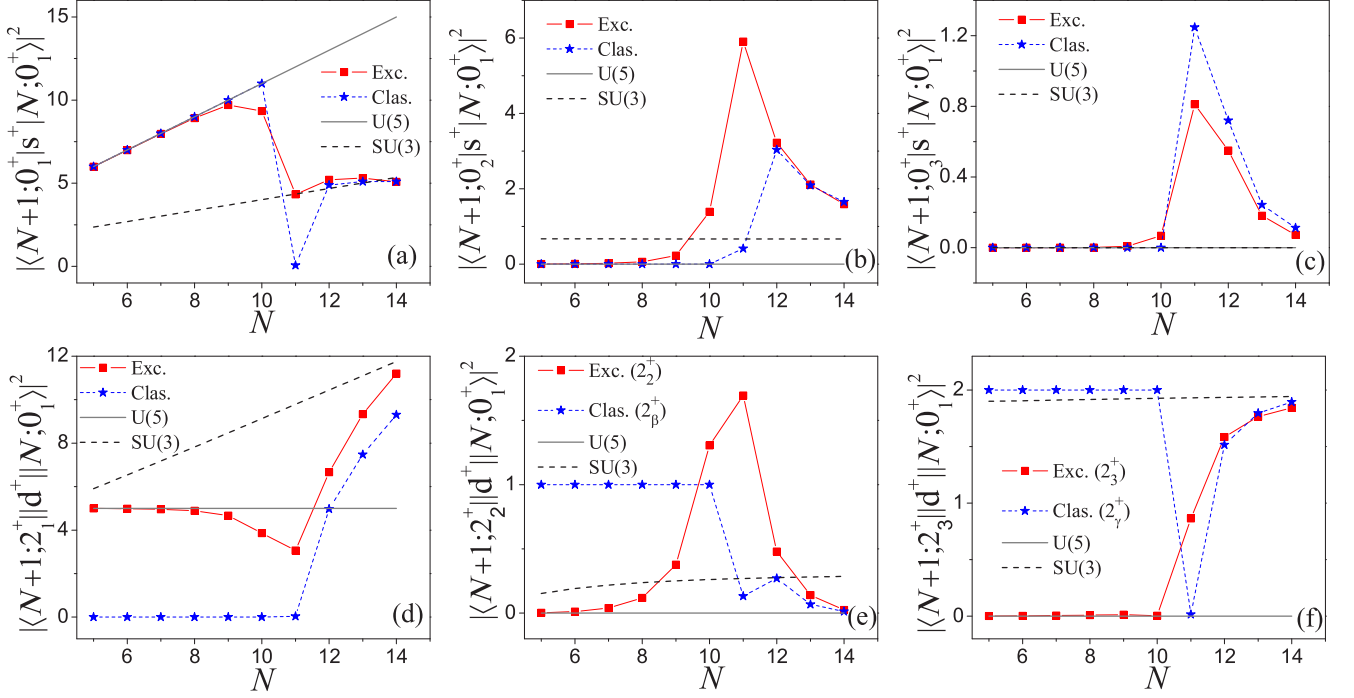
FIG. 4. Quantal-classical correspondence for the matrix elements of $s^\dagger$, $d_\mu^\dagger$ appropriate to (t,p) reaction intensities.

TABLE I. Parameters adopted in calculations for the Gd isotopes. Deduced parameters are separated by a line.

Neutron number	84	86	88	90	92	94	96	98
(η, χ)	$(0.27, -1.32)$	$(0.3, -1.32)$	$(0.41, -1.32)$	$(0.59, -1.1)$	$(0.72, -0.86)$	$(0.75, -0.8)$	$(0.84, -0.53)$	$(0.98, -0.3)$
ε_0 (in MeV)	1.272	1.127	0.92	1.204	1.469	1.499	1.612	1.794
ε_d (in MeV)	0.928	0.789	0.543	0.494	0.411	0.375	0.258	0.036
κ (in MeV)	0.0107	0.0094	0.0094	0.0161	0.0220	0.0216	0.02418	0.0293

TABLE II. Same as Table I but for the Sm isotopes.

Neutron number	84	86	88	90	92	94	96	98
(η, χ)	$(0.45, -0.3)$	$(0.48, -1.0)$	$(0.49, -1.2)$	$(0.6, -1.22)$	$(0.69, -1.24)$	$(0.71, -1.32)$	$(0.73, -1.32)$	$(0.75, -1.32)$
ε_0 (in MeV)	1.736	1.735	1.308	1.284	1.410	1.463	1.559	1.667
ε_d (in MeV)	0.955	0.902	0.667	0.513	0.437	0.452	0.421	0.416
κ (in MeV)	0.0279	0.026	0.0178	0.0192	0.0221	0.0231	0.0219	0.0223

TABLE III. Same as Table I but for the Nd isotopes.

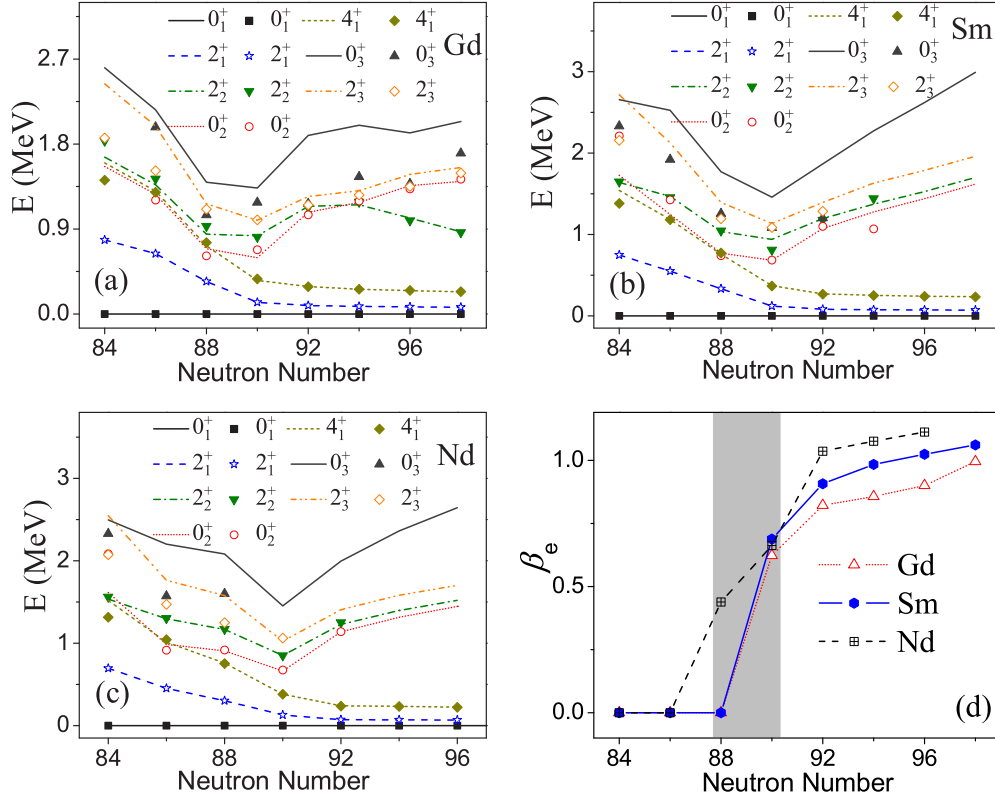| Neutron number	84	86	88	90	92	94	96
(η, χ)	$(0.45, -0.3)$	$(0.46, -1.32)$	$(0.568, -1.0)$	$(0.632, -1.0)$	$(0.75, -1.32)$	$(0.77, -1.32)$	$(0.79, -1.32)$
ε_0 (in MeV)	1.540	1.416	1.570	1.163	1.203	1.319	1.385
ε_d (in MeV)	0.847	0.765	0.68	0.428	0.301	0.303	0.291
κ (in MeV)	0.029	0.023	0.028	0.020	0.0226	0.0231	0.0228

FIG. 5. Comparison between the experimental (symbols) energies of the low-lying levels in the Gd, Sm, and Nd nuclei [15–24] and the calculated (lines) energies with the Hamiltonian (18). The calculated β_e values as a function of neutron number are given in panel (d).

TABLE IV. Available experimental data for (p,t) cross sections in the even Gd isotopes (units μb/sr) [29]. As indicated in [29], the relative errors within each nucleus are about 7% for the strong transitions ($>10\,\mu$b/sr) and 25% for the weak transitions ($<10\,\mu$b/sr).

$A+1 \to A$	$152 \to 150$	$154 \to 152$	$156 \to 154$	$158 \to 156$	$160 \to 158$	$\theta_{\mathrm{Lab}}^{\circ}$
$0_1 \to 0_1$	540	308	570	624	586	30
$0_1 \to 0_2$	60	274	90	64	$\leqslant 1$	30
$0_1 \to 0_3$	8	100	–	12	–	30
$0_1 \to 2_1$	26	169	290	295	259	5
$0_1 \to 2_2$	<1	64	40	30	–	5
$0_1 \to 2_3$	–	67	70	65	–	5

TABLE V. Available experimental data for (t,p) cross sections in the even Gd isotopes (units μb/sr) [30–32]. Although not explicitly indicated, an uncertainty of 7% have been given to the strong transitions ($>10\,\mu$b/sr) and 25% to the weak transitions ($<10\,\mu$b/sr) as in the (p,t) reactions shown above.

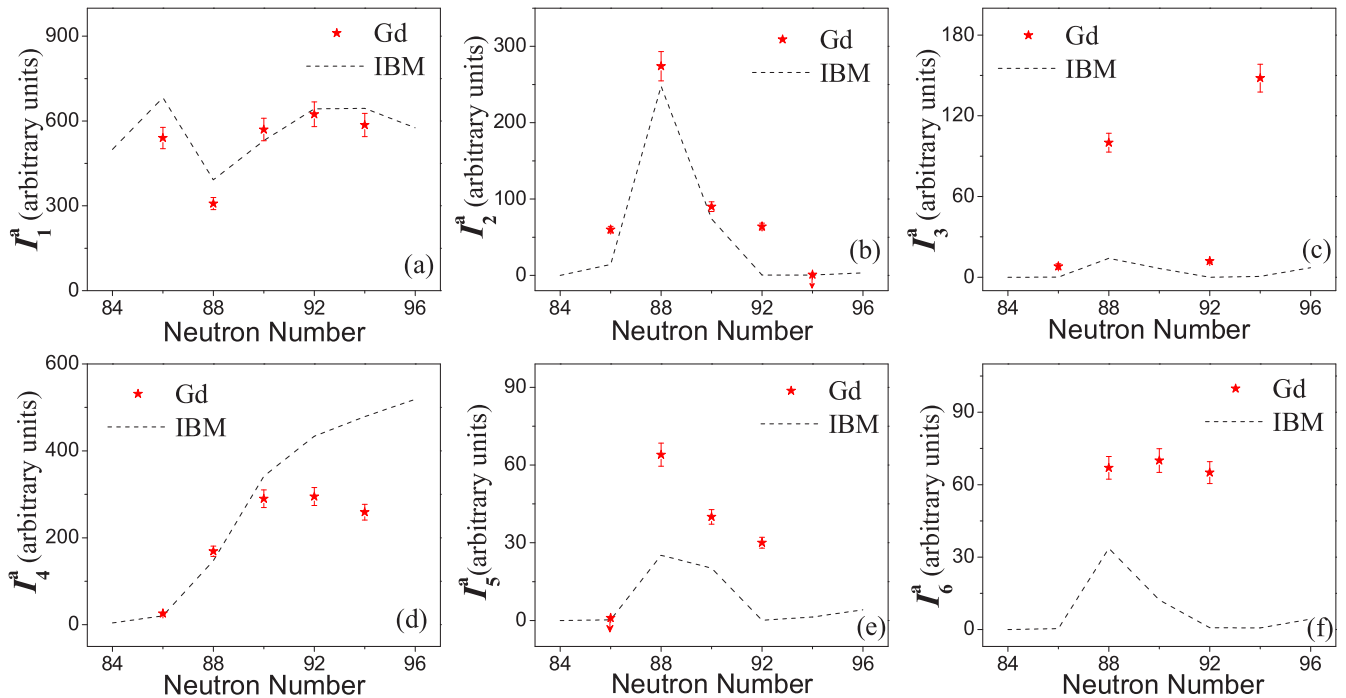| $A \to A+1$	$152 \to 154$	$154 \to 156$	$156 \to 158$	$158 \to 160$	$160 \to 162$	$\theta_{\mathrm{Lab}}^{\circ}$
$0_1 \to 0_1$	267	290	255	233	188	30
$0_1 \to 0_2$	162	3	20	–	39	30
$0_1 \to 0_3$	138	50	5	22	18	30
$0_1 \to 2_1$	17	11	24	21	19	30
$0_1 \to 2_2$	9	–	–	4	3	30
$0_1 \to 2_3$	–	3	–	–	–	60

FIG. 6. Comparison between calculated and experimental (p,t) transfer intensities for Gd. Here the values of the overall scale parameters t_{a_v} and t_{b_v} in the transfer operators are obtained by fitting the experimental data and given as $t_{a_v} = t_{b_v} = 3.46$ (arbitrary units).

the quantal matrix elements of the operator $d^\dagger$ have, in the spherical phase, a nonzero but finite value and appear to be of the same order of magnitude of the classical matrix elements in the deformed phase. However, this is a finite N effect, since in the figure only the classical values up to $N = 14$

are plotted. The squared classical matrix elements diverge as N for $N \to \infty$, which indicates that the relative discrepancy between the classical and exact results shown in Fig. 4(d) could be ignored in the large-N limit. Also it should be noted that the matrix elements of $s, d_\mu, s^\dagger, d_\mu^\dagger$ can be evaluated explicitly
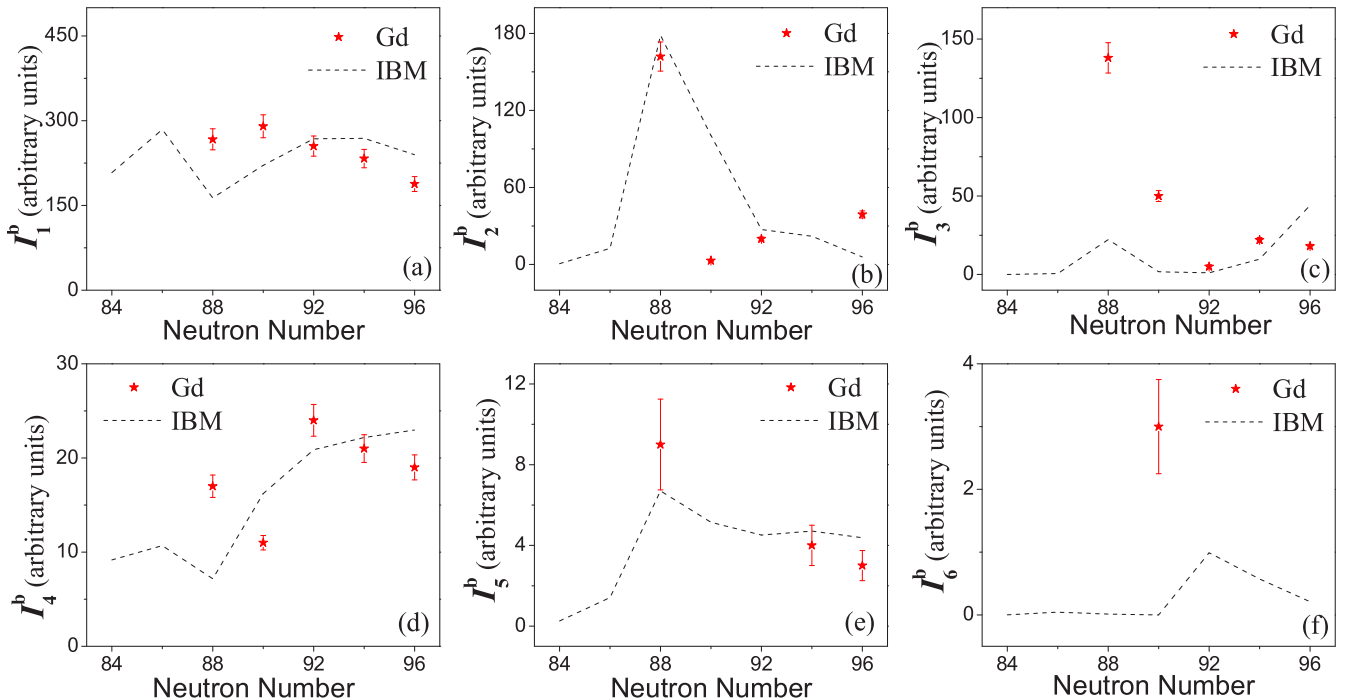

FIG. 7. Comparison between calculated and experimental (t,p) transfer intensities for Gd. Here the values of the overall scale parameters t_{a_v} and t_{b_v} in the transfer operators are obtained by fitting the experimental data and given as $t_{a_v} = 2.24$ and $t_{b_v} = 0.63$ (arbitrary units).

TABLE VI. Available experimental data for (p,t) cross sections in the even Sm isotopes, σ_{max}(units μb/sr) [33]. * denotes data measured at $\theta_{Lab}^{\circ} = 12\frac{1}{2}^{\circ}$ and † denotes data measured at $\theta_{Lab}^{\circ} = 30^{\circ}$. The relative errors for the transition $A+1 \rightarrow A$ with $A = 146, 148, 150, 152$ are assumed to be 3.0%, 13.0%, 6.9%, 3.9% [33].

$A+1 \rightarrow A$	$148 \rightarrow 146$	$150 \rightarrow 148$	$152 \rightarrow 150$	$154 \rightarrow 152$	θ_{Lab}°
$0_1 \rightarrow 0_1$	986	1166	488	739	25
$0_1 \rightarrow 0_2$	–	217	414	243†	25
$0_1 \rightarrow 0_3$	–	12	278	–	25
$0_1 \rightarrow 2_1$	52	82	162	285	10
$0_1 \rightarrow 2_2$	13	–	68	65	10
$0_1 \rightarrow 2_3$	23*	–	75	54*	10

TABLE VII. Available experimental data for (t,p) cross sections in the even Sm isotopes (units μb/sr) [34]. An uncertainty of 25% is given to each transition [34].

$A \rightarrow A+1$	$148 \rightarrow 150$	$150 \rightarrow 152$	$152 \rightarrow 154$	$154 \rightarrow 156$	$\theta_{c.m.}^{\circ}$
$0_1 \rightarrow 0_1$	570	190	300	300	27.8
$0_1 \rightarrow 0_2$	140	140	30	20	27.8
$0_1 \rightarrow 0_3$	–	130	100	–	27.8
$0_1 \rightarrow 2_1$	170	40	140	150	5.1
$0_1 \rightarrow 2_2$	50	50	–	40	5.1
$0_1 \rightarrow 2_3$	–	–	–	–	5.1

in the symmetry limits U(5) and SU(3) [9]. For example, the matrix elements of s for ground to ground transition are given by

$$U(5): |\langle N; g|s|N+1; g'\rangle|^2 = N+1 \tag{54}$$

$$SU(3): |\langle N; g|s|N+1; g'\rangle|^2 = (N+1)\frac{2N+3}{3(2N+1)}. \tag{55}$$

These limiting values are also shown in Figs. 3 and 4.

III. COMPARISON TO EXPERIMENT

To test the features of the phase transitional behavior of two-nucleon transfer intensities, we analyzed experiments in Gd, Sm, and Nd [15–24]. To this end, we first diagonalized the Hamiltonian, Eq. (18), using the program IBAR [25]. The three parameters ε_0, η, χ are obtained for each nucleus by fitting the low-lying levels. For comparison to previous calculations one

may also consider the deduced parameters in the consistent-Q parametrization [26]

$$\hat{H} = \varepsilon_d \hat{n}_d - \kappa \hat{Q}^\chi \cdot \hat{Q}^\chi$$

$$\varepsilon_d = \varepsilon_0(1-\eta), \quad \kappa = \varepsilon_0\eta/4N. \tag{56}$$

With the wave functions so obtained, we calculate the intensities of two-neutron transfer reactions using the operators of Sec. II.

The parameters ε_0, η, χ are given in Table I for Gd, II for Sm and III for Nd. In the tables we show also the deduced parameters ε_d, κ. Those for Gd were already given in [11]. A comparison to the experiments is given in Fig. 5. One can see that the Hamiltonian (18) provides an excellent description of the energies except for the state 0_3^+. Several suggestions have been made for the nature of this state, including a mixed symmetry state [27] and an additional degree of freedom, s' boson [28], related to a pair-vibration. In Fig. 5(d) the
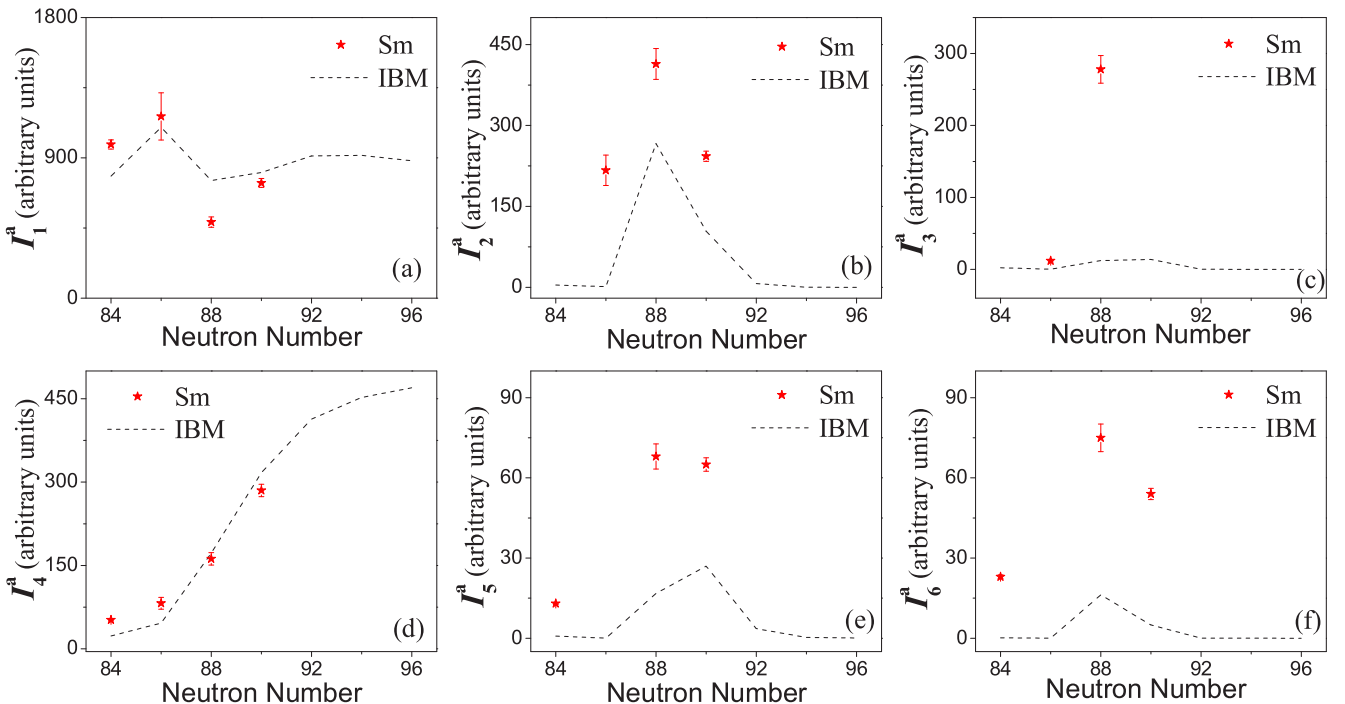

FIG. 8. Comparison between calculated and experimental (p,t) transfer intensities for Sm. Here the values of the overall scale parameters t_{a_ν} and t_{b_ν} in the transfer operators are obtained by fitting the experimental data and given as $t_{a_\nu} = 4.47$ and $t_{b_\nu} = 3.16$ (arbitrary units).
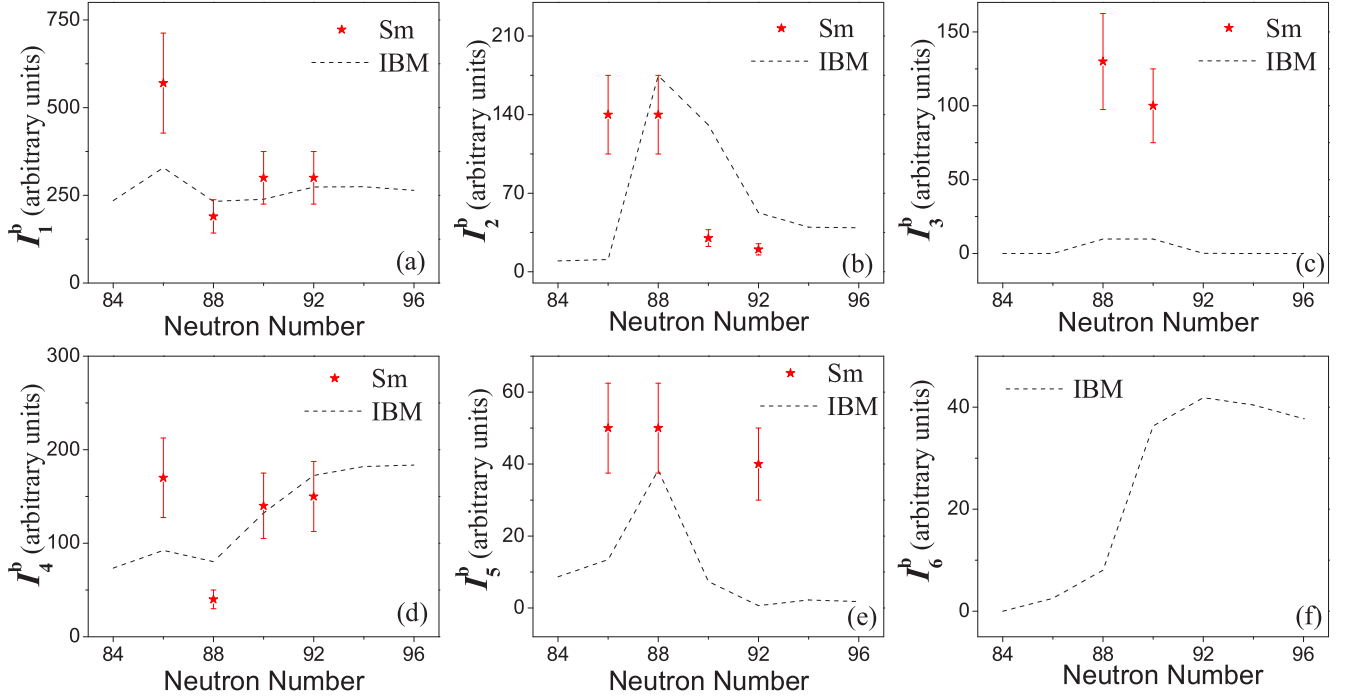
FIG. 9. Comparison between calculated and experimental (t,p) transfer intensities for Sm. Here the values of the overall scale parameters in the transfer operators are obtained by fitting the experimental data and given as $t_{a_\nu} = 2.45$ and $t_{b_\nu} = 1.73$ (arbitrary units).

calculated values of β_e are also shown as a function of neutron number. These values show clearly a transitional behavior. These values must be multiplied by a scale to convert them to the Bohr definition (see [9], p. 105).

A. Gd nuclei

Experimental data for (p,t) and (t,p) reactions are given in Tables IV and V. The angle $\theta_{\text{Lab}}^\circ$ at which the cross section was measured is also given for clarity. A comparison to calculations is shown in Figs. 6 and 7. From these figures one can see that intensities to $0_1^+, 2_1^+, 0_2^+, 2_2^+$ are well described by the calculations, especially for (p,t) reactions as shown in Figs. 6(a), 6(b), 6(d), and 6(e), where the transitional signatures around the neutron number $N_n = 90$ clearly appear in both theory and experiment. In contrast, those corresponding to 0_3^+ and 2_3^+ in experiments cannot be well reproduced by the calculations, which is actually consistent with the conclusion drawn from Fig. 5(a).

TABLE VIII. Available experimental data for (p,t) cross sections in the even Nd isotopes (units μb/sr) [35]. Errors quoted in [35] are shown in parentheses.

$A \rightarrow A+1$	$146 \rightarrow 144$	$148 \rightarrow 146$	$\theta_{\text{Lab}}^\circ$
$0_1 \rightarrow 0_1$	639(5)	827(12)	10
$0_1 \rightarrow 0_2$	28(1)	–	10
$0_1 \rightarrow 0_3$	4(0.4)	–	10
$0_1 \rightarrow 2_1$	9.2(0.6)	98(4)	10
$0_1 \rightarrow 2_2$	37(1)	3.6(0.8)	10
$0_1 \rightarrow 2_3$	33(1)	10(1)	10

B. Sm nuclei

The parameters ε_0, η, χ in the Hamiltonian for these nuclei are given in Table II. Experimental data for (p,t) and (t,p) reactions are given in Tables VI and VII, and compared to the calculation in Figs. 8 and 9. Similarly, it can be found from these figures that the phase transitional features in the Sm isotopes for the lowest $0^+, 2^+$ states can be generally well produced by the theoretical calculations, while for those corresponding to 0_3^+, the calculated transitional amplitudes around $N_n = 90$ are evidently smaller than those present in experiments as those in the Gd isotopes, which further suggests that partial 0_3^+ and 2_3^+ states in these deformed rare-earth nuclei cannot be accommodated by the present model space.

C. Nd nuclei

The parameter ε_0, η, χ for Nd are given in Table III. A conclusion similar to that in Gd and Sm can be drawn here for the state 0_3^+. Experimental data for (p,t) and (t,p) reactions

TABLE IX. Available experimental data for (t,p) cross sections in the even Nd isotopes [36]. The results have been normalized to that for $0_1 \rightarrow 0_1$ in each case. Although not explicitly indicated, an uncertainty of 25% is given to each (t,p) transition as in Table VII.

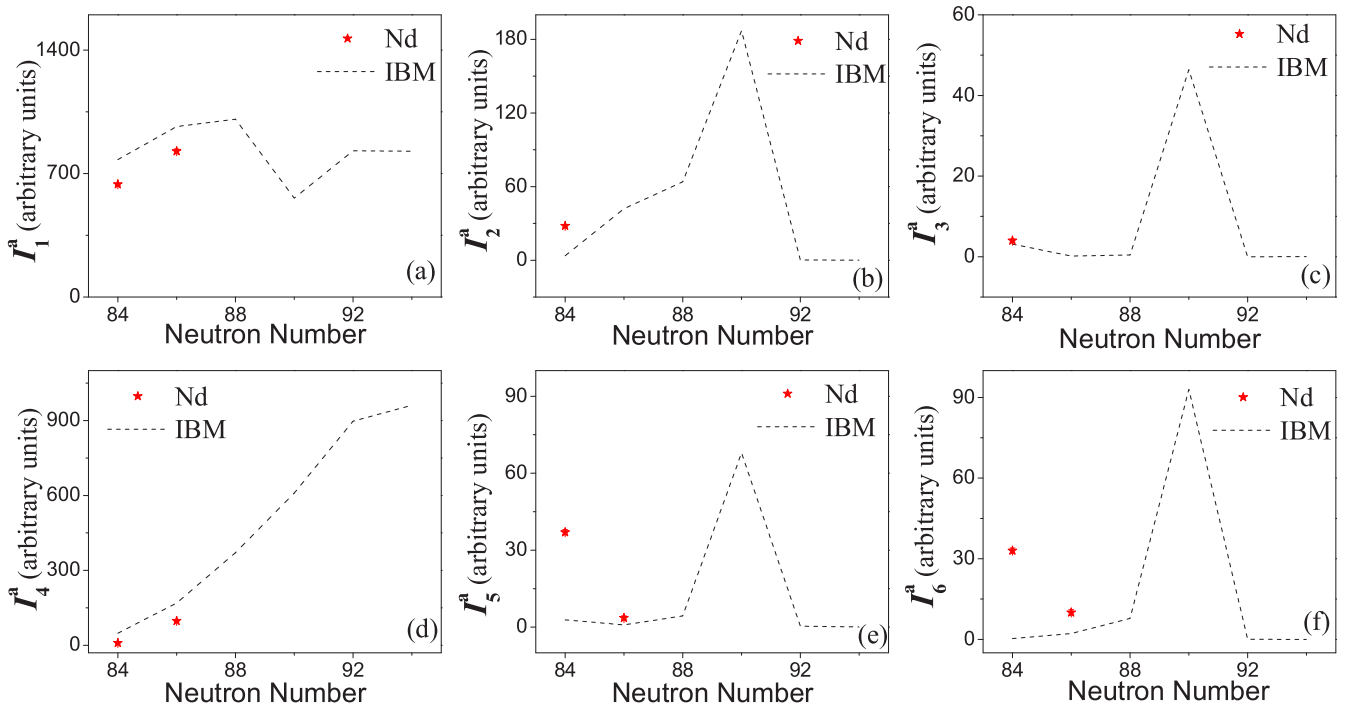| $A \rightarrow A+1$	$144 \rightarrow 146$	$146 \rightarrow 148$	$148 \rightarrow 150$	$150 \rightarrow 152$	$\theta_{\text{c.m.}}^\circ$
$0_1 \rightarrow 0_1$	100	100	100	100	27.8
$0_1 \rightarrow 0_2$	–	15	128	72	27.8
$0_1 \rightarrow 0_3$	–	–	–	–	–
$0_1 \rightarrow 2_1$	45	46	55	40	5.1
$0_1 \rightarrow 2_2$	–	30	53	58	5.1
$0_1 \rightarrow 2_3$	–	–	–	–	–

FIG. 10. Comparison between calculated and experimental (p,t) transfer intensities for Nd. Here the values of the overall scale parameters in the transfer operators are obtained by fitting the experimental data and given as $t_{a_v} = t_{b_v} = 5.48$ (arbitrary units).

are given in Tables VIII and IX. A comparison to the calculated (p,t) intensities is shown in Fig. 10, where only several data for spherical N_d nuclei are available in experiments. In Fig. 11,

we show instead a comparison to the calculated (t,p) ratios of intensities since only intensities relative to the ground state were reported in experiments. [36].
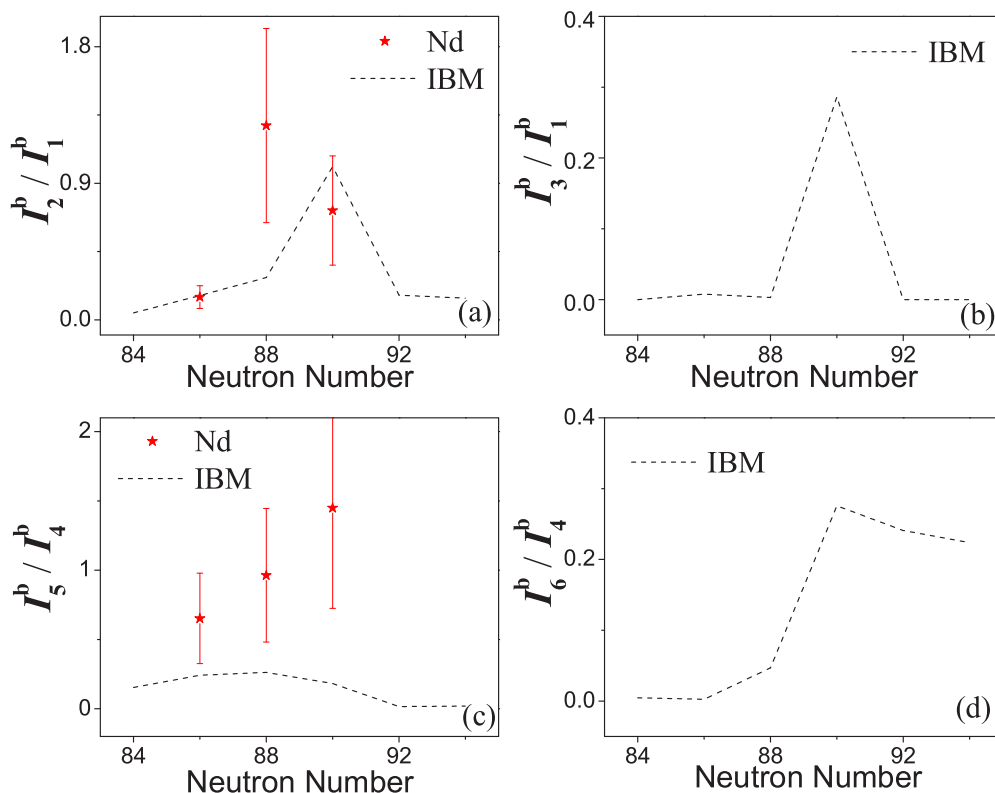

FIG. 11. Comparison between calculated and experimental (t,p) transfer intensities ratios for Nd. Ratios are independent of scale parameter.

IV. SUMMARY AND CONCLUSION

In this work, a systematical analysis of the two-neutron transfer intensities as a possible signature of the U(5)–SU(3) shape phase transition has been carried in the IBM in both a classical way and exactly numerical calculation. Specifically, the classical elements of the two-nucleon transfer operator related to the low-lying 0^+ and 2^+ states are derived and the resulting phase transitional characteristics have been revealed through the quantal-classical correspondence. Experimental data of two-neutron transfer intensities in Gd, Sm, and Nd show clear evidence for the occurrence of a quantum phase transition between spherical [U(5)) and axially deformed (SU(3)] shape, in agreement with previous studies of two-neutron separation energies, S_{2n}, electromagnetic transition rates, $B(E2; 2_1^+ \rightarrow 0_1^+)$, and energy ratios $E(4_1^+)/E(2_1^+)$. The evidence is particularly clear for the intensity $I(N+1, 0_1^+ \rightarrow N, 2_1^+)$, which is proportional to the square of the order parameter β_e^2. Transitions to 0_1^+, 2_1^+, 0_2^+, 2_2^+ states follow closely the expected behavior for the phase transition both in (p,t) and (t,p) reactions. Transitions to 0_3^+ and 2_3^+ do not follow the expected behavior indicating that these states are outside the model space of IBM-1 used in this article.

Two-nucleon transfer reactions appear to be an excellent tool to test phase transitional behavior, since they are sensitive to the deformation of the initial and final state and to their differences. This result was already given in [8] and it is strengthened by the present calculations. Finally, the study reported here can be extended to two-proton transfer reactions, and two-proton and two-neutron transfer reactions.

[1] P. Cejnar and J. Jolie, Prog. Part. Nucl. Phys. **62**, 210 (2009).

[2] P. Cejnar, J. Jolie, and R. F. Casten, Rev. Mod. Phys. **82**, 2155 (2010).

[3] F. Iachello and M. A. Caprio, in *Understanding Quantum Phase Transitions*, edited by L. D. Carr (CRC, Boca Raton, FL, 2011), pp. 673–700.

[4] F. Iachello, Riv. Nuovo Cimento **34**, 617 (2011).

[5] F. Iachello, Phys. Rev. Lett. **85**, 3580 (2000).

[6] F. Iachello, Phys. Rev. Lett. **87**, 052502 (2001).

[7] F. Iachello and N. V. Zamfir, Phys. Rev. Lett. **92**, 212501 (2004).

[8] R. Fossion, C. E. Alonso, J. M. Arias, L. Fortunato, and A. Vitturi, Phys. Rev. C **76**, 014316 (2007).

[9] F. Iachello and A. Arima, *The Interacting Boson Model* (Cambridge University Press, Cambridge, England, 1987).

[10] A. Arima and F. Iachello, Phys. Rev. C **16**, 2085 (1977).

[11] E. A. McCutchan, N. V. Zamfir, and R. F. Casten, Phys. Rev. C **69**, 064306 (2004).

[12] R. Bijker and A. E. L. Dieperink, Phys. Rev. C **26**, 2688 (1982).

[13] A. Leviatan, Z. Phys. A **321**, 467 (1985).

[14] P. Van Isacker and J. Q. Chen, Phys. Rev. C **24**, 684 (1981).

[15] A. A. Sonzogni, Nucl. Data Sheets **93**, 599 (2001).

[16] L. K. Peker and J. K. Tuli, Nucl. Data Sheets **82**, 187 (1997).

[17] N. Nica, Nucl. Data Sheets **117**, 1 (2014).

[18] S. K. Basu and A. A. Sonzogni, Nucl. Data Sheets **114**, 435 (2013).

[19] M. J. Martin, Nucl. Data Sheets **114**, 1497 (2013).

[20] C. W. Reich, Nucl. Data Sheets **110**, 2257 (2009).

[21] C. W. Reich, Nucl. Data Sheets **113**, 2537 (2012).

[22] R. G. Helmer, Nucl. Data Sheets **101**, 325 (2004).

[23] C. W. Reich, Nucl. Data Sheets **105**, 557 (2005).

[24] C. W. Reich, Nucl. Data Sheets **108**, 1807 (2007).

[25] R. J. Casperson, Comput. Phys. Commun. **183**, 1029 (2012).

[26] D. D. Warner and R. F. Casten, Phys. Rev. C **28**, 1798 (1983).

[27] O. Scholten, K. Heyde, P. Van Isacker, and T. Otsuka, Phys. Rev. C **32**, 1729 (1985).

[28] P. Van Isacker, K. Heyde, M. Waroquier, and G. Wenes, Nucl. Phys. A **380**, 383 (1982).

[29] D. G. Fleming, C. Günther, G. Hagemann, B. Herskind, and Per O. Tojm, Phys. Rev. C **8**, 806 (1973).

[30] M. A. M. Shahabuddin, D. G. Burke, I. Nowikow, and J. C. Waddington, Nucl. Phys. A **340**, 109 (1980).

[31] G. Lovhoiden, T. F. Thorsteinsen, E. Andersen, M. F. Kiziltan, and D. G. Burke, Nucl. Phys. A **494**, 157 (1989).

[32] G. Lovhoiden, T. F. Thorsteinsen, and D. G. Burke, Phys. Scr. **34**, 691 (1986).

[33] P. Debenham and N. M. Hintz, Nucl. Phys. A **195**, 385 (1972).

[34] J. H. Bjerregaard, O. Hansen, O. Nathan, and S. Hinds, Nucl. Phys. **86**, 145 (1966).

[35] V. Yu. Ponomarev, M. Pignanelli, N. Blasi, A. Bontempi, J. A. Bordewijk, R. De Leo, G. Graw, M. N. Harakeh, D. Hofer, M. A. Hofstee, S. Micheletti, R. Perrino, and S. Y. van der Werf, Nucl. Phys. A **601**, 1 (1996).

[36] R. Chapman, W. McLatchie, and J. E. Kitching, Nucl. Phys. A **186**, 603 (1972).